THE EFFECTIVENESS OF VISCOUS DAMPERS FOR STRUCTURES SUBJECTED TO LARGE EARTHQUAKES

H. Kit Miyamoto and Amir SJ Gilani
Miyamoto International, Sacramento, CA, USA

Akira Wada
Tokyo Institute of Technology, Tokyo Japan

SUMMARY
The efficacy of dampers in providing seismic protection has been validated by the excellent performance of buildings fitted with dampers in the past earthquakes. However, previous studies have not accounted for the limit states of dampers. Recently, a multi-year research project was completed that investigated the seismic performance of building with dampers subject to large earthquakes. It was shown that the limit states of viscous dampers have a significant effect on the response of the building. Experimental data from laboratory tests of viscous dampers were used to calibrate a model of viscous dampers with limit states. Next, analytical model of steel buildings with viscous dampers, incorporating damper limit states, were prepared and analyzed to determine their collapse performance. Analysis showed excellent performance and revealed that, the use of factors of safety to delay the onset of reaching limit states was beneficial.

Keywords: Fluid viscous dampers, limit state model, nonlinear analysis, steel archetypes, collapse probability

1 INTRODUCTION

Viscous dampers were originally developed as shock absorbers for the defense and aerospace industries. In re-cent years, they have been used extensively for seismic application for both new and retrofit construction. During seismic events, the devices become active and the seismic input energy is used to heat the fluid and is thusly dissipated. Subsequent to installation, the dampers require minimal maintenance. They have been shown to possess stable and dependable properties for design earthquakes. Figure 1 depicts the application of dampers to a new building in California (Miyamoto and Gilani, 2008).

Viscous dampers consist of a cylinder and a stainless steel piston. The cylinder is filled with incompressible silicone fluid. The damper is activated by the flow of silicone fluid between chambers at opposite ends of the unit, through small orifices. Figure 2 shows the damper cross section.

Figure 1. Steel moment frame with dampers

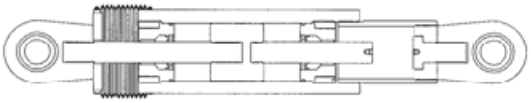

Figure 2. Viscous damper cross section

2 MODELING OF VISCOUS DAMPERS

2.1 Overview

In most applications, the dampers are modeled as simple Maxwell model of Figure 3. The viscous damper itself is modeled as a dashpot in series with the elastic driver brace member. Such model is adequate for most design applications, but is not sufficiently refined for collapse evaluation. In particular, force and displacement limit states are unaccounted.

Although dampers are comprised of many parts, the limit states are governed by a few elements. The dampers bottoms out, once the piston motion reaches its available stroke. This is the stroke limit and results in transition from viscous damper to a steel brace with stiffness equal to that of the cylinder wall. The force limit states in compression and tension are governed by the buckling capacity of the driver brace and the tensile capacity of the piston rod, respectively.

Figure 4 presents the proposed refined model for viscous dampers. This model is developed to incorporate the pertinent limit states and consists of five components. The constitutive relation for the refined model in terms of force, velocity, and displacement is listed in (Eq 1)

$$\Delta u = \frac{\Delta F}{K_D(u)} + \frac{\Delta F}{K_P(u)} + \begin{Bmatrix} \frac{\Delta F}{K_C} \text{.....} |u| > u_{\max} \\ \operatorname{sgn}(F)\frac{1}{C^{\alpha}}\int |F|^{1/\alpha} dt \end{Bmatrix}$$
$$\Delta F = 0 \text{...} |F| \geq F u_P \qquad (1)$$

The damper components are modeled as following: a) the driver used to attach the damper to the beams and columns is modeled as a nonlinear spring, b) the piston rod and undercut is modeled as a nonlinear spring. The piston undercut is the machined down section between the end of the piston and the start of the piston male threaded part. In tension, the undercut section of the piston can yield and fracture, c) dashpot is used to model the viscous component, d) gap element and linear springs (are used to model the limit state when the piston retraction equals the stroke). The elastic stiffness depends on the damper construction and its cylinder properties, e) hook elements and linear springs are used to model the limit state when the piston extension reaches the damper stroke. The stiffness is the same as that associated with the gap element.

2.2 Response of the Limit State Model

In analysis, once the stroke limit is reached, the damper becomes numerically equivalent to a steel brace. Upon unloading, this process is reversed. When the force limit is reached, the entire damper is

ineffective and thus permanently removed, even after unloading. The sudden transmissions between viscous damper, steel brace, and no members can impart large impact forces on the structure. At the instant that the gap closes, the damper force is zero. However, as loading is continued, the unit displacement can increase due to deformation in the cylinder wall and thus velocity is non-zero. At the large peaks, the damper force, which is algebraic sum of the force in the dashpot and the cylinder wall, can be smaller than the force resisted by the wall cylinders. This is because the forces in the viscous element and cylinder wall can be out-of-phase.

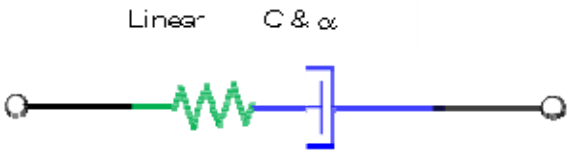

Figure 3. Maxwell model

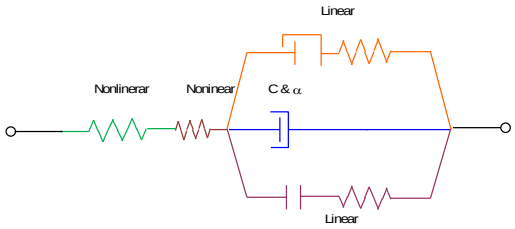

Figure 4. Limit state model

2.3 ANALYTICAL SIMULATIONS

To illustrate the response of the refined model and illustrate its capability to capture all the limit states, simulations were conducted. The damper was modeled in program OpenSees (PEER 2009a) using the refined model. All analysis was conducted using a sinusoidal displacement loading function. The damper used in simulation is the 700-kN unit and has a constitutive relation (force in kN and velocity in mm/sec) of Eq. 2

$$F = 88\,\mathrm{sgn}(v)|v|^{0.3} \tag{2}$$

2.3.1 Displacement and force limits

The stroke limit is reached first. If the loading is increased, then the driver will buckle in tension or undercut will yield and fracture in tension. This simulation was conducted to investigate the damper response for the limit state of piston fracture following bottoming out of damper at full extension. The response is shown in Figure 5. At 4.5 sec in the response, the piston extension reaches the stroke limit and the damper bottoms out. At this point, velocity is zero and thus the force in the viscous element drops to zero. The damper acts as an elastic brace. The undercut yields but does not fracture. Loading is then reversed. This results in the disengagement of cylinder walls, and re-loading of the viscous component. At 5.3 sec, piston bottoms out again. The damper again becomes an elastic brace. Loading is increased further resulting in fracture of undercut.

2.3.2 Response to Earthquake Acceleration

The damper was next subjected to the 1994 Kobe record to assess its performance of the damper. The unsealed input acceleration is shown in Figure 6a, and was used as acceleration input along the axis of the damper element. Figure 6b presents the response at 100% intensity. Note that the response is that of the pure viscous damper and no limit states are reached. Next the record was amplified to 125% and the response is shown in Figure 6c. Even such modest amplification, resulted in the damper reaching its displacement limit and bottoming out in both tension and compression. Once damper bottomed, large elastic forces (twice the maximum viscous force) were generated and which must be resisted by steel members in structural applications. Finally, the force limit state was reached when the record was amplified by 175%; see Figure 6d. This is not a large scaling. The damper bottomed out in compression twice, followed by bottoming in tension which leads to the yielding, and fracture

of piston undercut. After this point, the damper is completely ineffective. In structural applications, this implies removal of beneficial supplementary energy from the system.

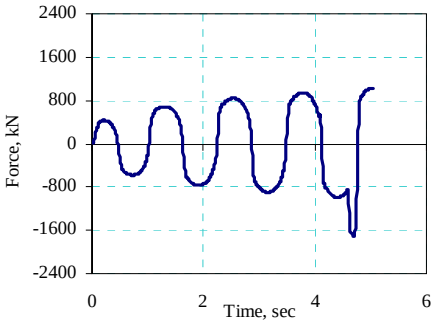

a. Damper

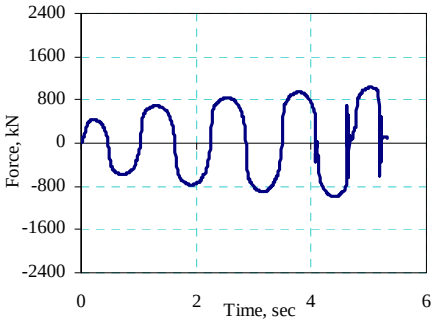

b. Viscous element

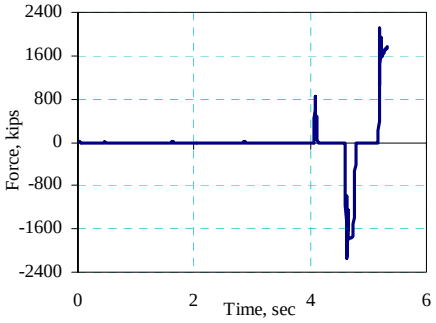

c. Gap/hook element and cylinder walls

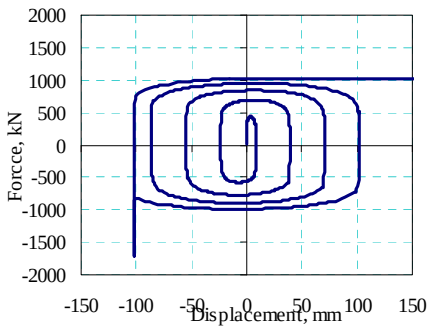

d. Damper hysteresis

Figure 5. Response for compound case

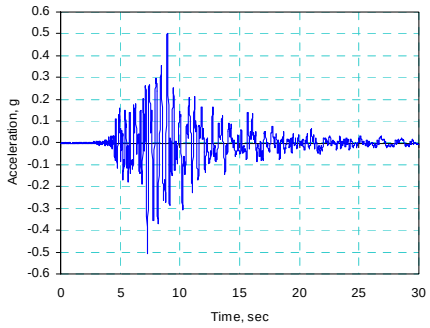

a. Input acceleration

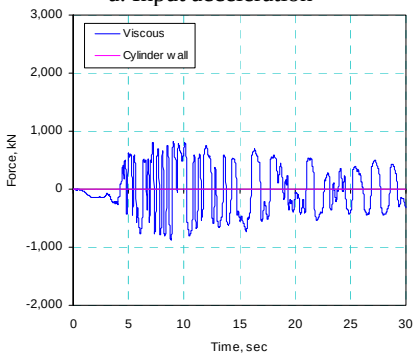

b. Response, 100% event

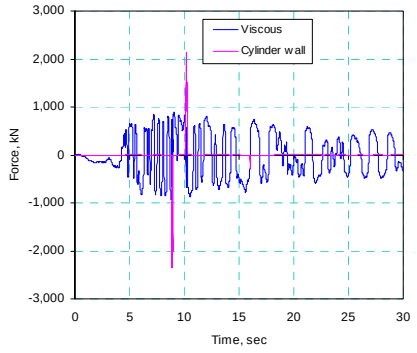

c. Response, 125% event

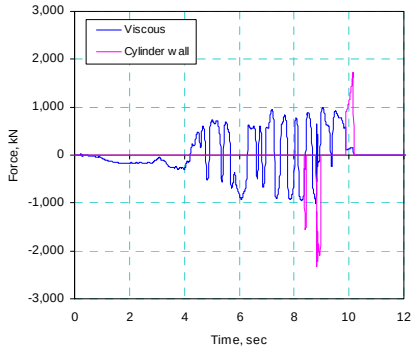

d. Response, 175% event

Figure 6. Response to amplified Kobe record

2.4 Correlation with Laboratory Testing

Experimental data from a damper (Taylor, 2009) was used to assess the accuracy of the mathematical model of dampers. This damper had a constitutive relation (force in kips and velocity in in./sec), in the design range, is written as in Eq 3.

$$F = 3.5\, sgn(v)|v|^{0.5} \tag{3}$$

The damper was placed in the test rig and subject to a displacement loading history. The unit was placed with its piston extended to within 10 mm of the stroke limit prior to start of the displacement cycles. The experimental displacement, velocity, and force responses are presented as solid lines in Figure 7a through Figure 7c, respectively. The damper limit states are identified in this figure. At 4.3 sec, the unit was pulled in tension at 910 mm/sec and stopped just before it bottomed. This large velocity was close to 300% of its nominal design. This resulted in the forces developed in the damper that exceeded the nominal value computed from the constitutive relation. At 4.61 sec, the damper bottoms out in tension, resulting in sharp increase in the measured force. This is followed by tensile yielding. The displacement response after this point is nearly flat with a slight increase due to yielding. Finally at 4.68 sec, fracture occurs and the damper load drops to zero. After this time, no force can be transferred by the damper. The dashed lines in these figures represent the results obtain from simulation using the refined damper element. Good correlation is obtained between the experimental data and analytical simulations. The analytical model was able to capture the bottoming of the damper and tensile fracture correctly. Figure 7d presents the force-displacement hysteresis and the dissipated energy in the damper. The analytical model captures the experimental responses closely, implying that the analytical model is able to reproduce the energy dissipation properties of the laboratory-tested unit.

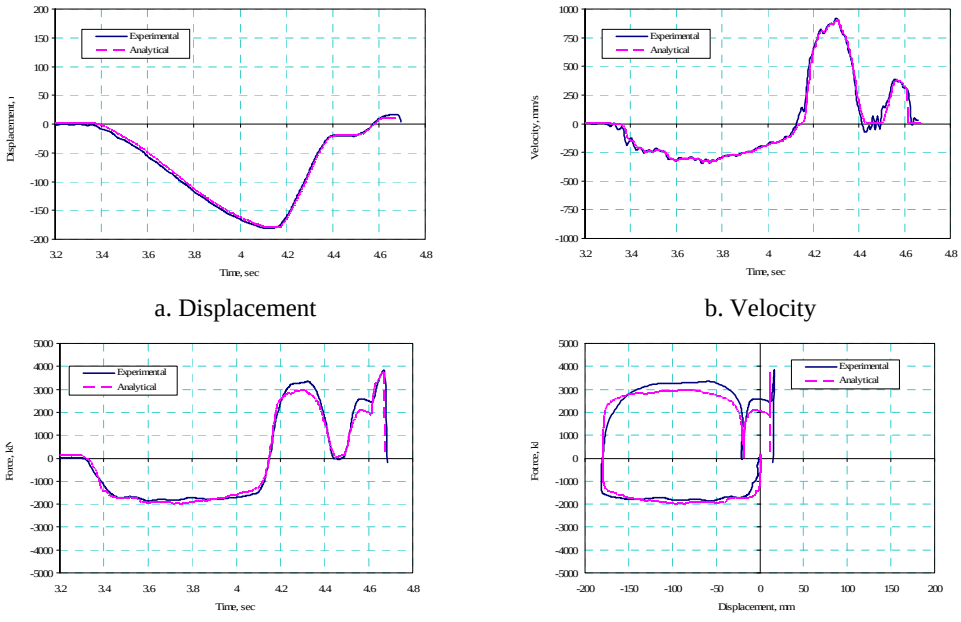

a. Displacement

b. Velocity

c. Force

d. Damper hysteresis

Figure 7. Experimental and analytical results

3 ANALYSIS PROCEDURE

3.1 Ground Motions

The input histories used in analysis were based on the two components of the 22 far-filed (measured 10 km or more from fault rupture) NGA PEER (2009b) records. These 44 records have been identified by ATC 63 (FEMA 2009) for collapse evaluation analysis. The selected 22 records correspond to a relatively large sample of strong recorded motions that are consistent with the code (ASCE/SEI 7) and are structure-type and site-hazard independent. Figure 8 presents the acceleration response spectra for these records. The design MCE spectrum is shown as the thick solid line in the figure. For analysis, the 44 records were first normalized and then scaled. Normalization of the records was done to remove the record-to-record variation in intensity.

3.2 SMRF Connection

Steel SMRFs with reduced beam sections (RBSs) are one of the prequalified connections for seismic applications and were used in this analysis. The constitutive post-yield relation for the RBS plastic hinges developed by Lignos (2008) was used in this subject study. Those authors used experimental data from a database of 42 RBS connections tested in laboratories using regression analysis; they identified the plastic hinge properties as a function of flange slenderness, web slenderness, lateral bracing, and yield strength of beams. The moment-rotational definitions, the multilinear moment-rotation constitutive relation for the RBS plastic hinges was thus defined. A sample hinge response is shown in Figure 9. FEMA 350 (FEMA 2000) recommends the introduction a reduction in the flexural stiffness to account for the effect of the reduced beam flanges. Such reduction will result in an increase in the story drifts by 3% to 7% in typical applications. FEMA 350 also recommends increasing story drifts by 10% to account conservatively for this effect. This approach was used to scale up the computed inelastic drifts:

3.3 Model Properties and IDA

Program OpenSees (PEER 2009a) was used to conduct the nonlinear analyses described in this paper. Pertinent model properties are listed here.

- Analytical models are two-dimensional
- Beam and column elements, are represented as one dimensional frame elements. Material nonlinearity is represented by concentrated plastic hinges represented by RBS hinges.
- The damper element is represented by the refined model including the limit states.

For collapse analysis, the normalized records are then scaled upward or downward to obtain data points for the nonlinear incremental dynamic analysis (IDA) simulations (Vamvatsikos and Cornell, 2004).

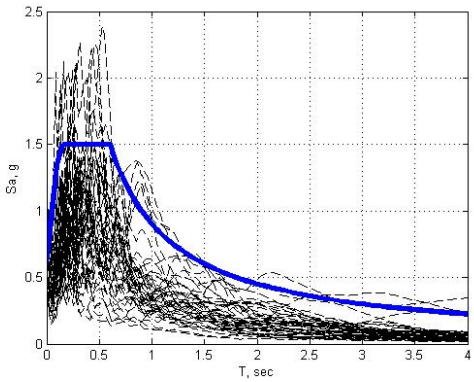

Figure 8. Response spectra of original records

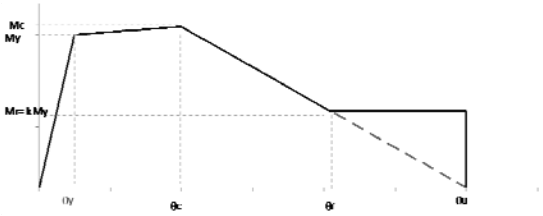

Figure 9. RBS hinge Moment-rotation relation

4 APPLICATION TO STEEL BUILDINGS

4.1 General

To illustrate the concepts described in this paper, design and analysis of a group of archetypes with viscous damping was conducted. Fifteen archetypes (from one to thirty story buildings) are currently under consideration. The basic geometry and distribution of dampers for these models are summarized in Table 1. The selected building models will be regular in plan and elevation with a dominant first mode response. The period of tall buildings is limited to approximately 5 sec to ensure sufficient energy is present in the input histories. The investigations for all but the 20- and 30-story structures have been completed. The frames were designed using the code provisions and special requirements for SMRFs. The ASCE 7 maximum period used to compute base shear period is used for evaluation. A typical 5-story archetype is shown in Figure 10.

Table 1. Archetypes

Archetype	Stories	Column base	Drift Ratio	Damper FS
O1	1	Pinned	2.5%	1.0
O2	1	Pinned	1.0%	1.3
O3	1	Fixed	2.5%	1.0
O4	1	Fixed	1.0%	1.3
A1	2	Pinned	2.5%	1.0
A2	2	Pinned	1.0%	1.3
A3	2	Fixed	2.5%	1.0
A4	2	Fixed	1.0%	1.3
B1	5	Fixed	2.0%	1.0
B2	5	Fixed	1.0%	1.3
C1	10	Fixed	2.0%	1.0
C2	10	Fixed	1.0%	1.3
D1	20	Fixed	2.0%	1.0
D2	20	Fixed	1.0%	1.3
E1	30	Fixed	1.0%	1.0

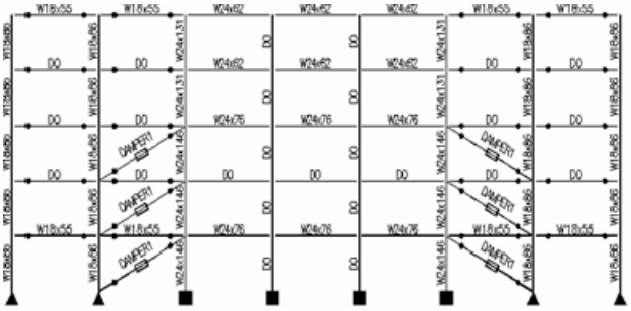

Figure 10. Five-story archetype B1

4.2 Damper property selection

Following the design of moment frames according to ASCE/SEI 7 requirements for strength, dampers were sized to limit story drift ratios. ASCE/SEI 7 presents recommendations for the design of dampers. This approach was used to provide an approximate damper size, assuming stiffness

proportional to damping. However, because dampers had a velocity coefficient (α of 0.5 and because they did not extend throughout the full building height, the damper constant was then computed more accurately by conducting nonlinear analysis at the design earthquake (DE) level. Three sets of spectrum-compatible records that matched the DE spectrum were developed. Northridge, Kobe, and Newhall records were used from the Pacific Earthquake Engineering Research Center (PEER) Next Generation Attenuation (NGA) database (PEER 2009b). Additionally, the Kobe record was scaled such that the ordinate of its response spectrum matched the DE spectrum at the building's fundamental period

5 ANALYSIS RESULTS

The analysis results for the five-story archetypes are presented in Figure 11. For the pushover curves, the solid and .dashed lines correspond to the cases where damper are excluded and included, respectively, in analysis. As long as the damper does not bottom out, the plots are identical. Once the damper bottoms, there is significant increase in stiffness and strength since a stiff brace (cylinder wall) is now added to the system. After the damper fails, the damped pushover curve asymptotically approaches the undammed case. The dotted line corresponds to a bilinear approximation used to compute the yield and ultimate drifts and the corresponding ductility (μc). The computed system ductility was 8.0 and resulted in a SSF of 1.34.

For the IDA plots, the solid and dashed red lines correspond to the MCE (SMT) and the median collapse capacity (SCT), respectively. Note that the addition of small damper factor of safety significantly increases collapse margin. For the fragility plots, the 44 collapse data are statiscally organized and a lognormal curve is filled to the data (dashed lines in the figures). The plot was then rotated to correspond to a total uncertainty of 0.55 (solid line) per FEMA P695. Finally the curve was shifted to account for the effect of the SSF (dark solid lines in the figures). The probability of collapse at MCE intensity was then be computed. The probability of collapse at MCE level was reduced by a factor of approximately 4 when an additional damper factor of safety of 30% is included. The probability of the damper reaching its limit state at the MCE intensity can then be computed from the damper fragility plots. Note that the probability of damper reaching a limit state is significantly reduced when a damper factor of safety of 30% is included in design.

Table 2 summarizes the analysis results. The collapse margin ratio (CMR) is defined as the ratio of SCT and SMT. The adjusted collapse margin ratio (ACMR) is then computed as the product of SSF and CMR. FEMA P695 specifies a minimum ACMR of 1.59 for acceptable performance. Both archetypes have significantly larger collapse margins and therefore pass easily.

Table 2. Damper fragility data

							Response probability at MCE	
Archetype	SCT	SMT	CMR	SSF	ACMR	P/F	collapse	Damper capacity
B1	1.24	0.82	1.51	1.34	2.20	Pass	8.0%	22%
B2	1.81	0.82	2.25	1.34	3.10	Pass	2.0%	10%

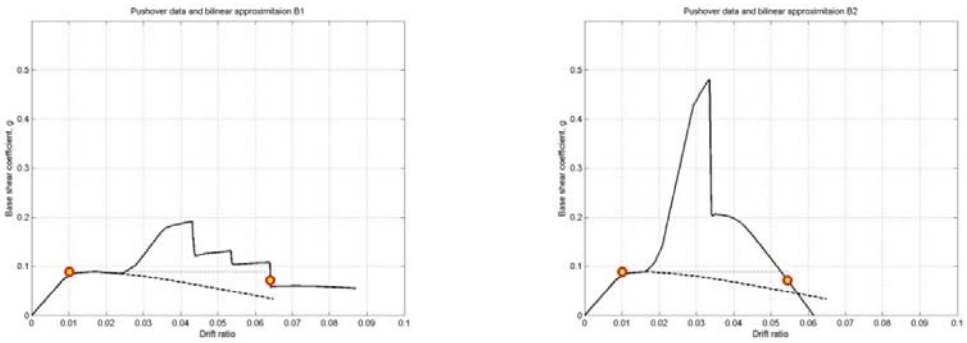

Static pushover curves

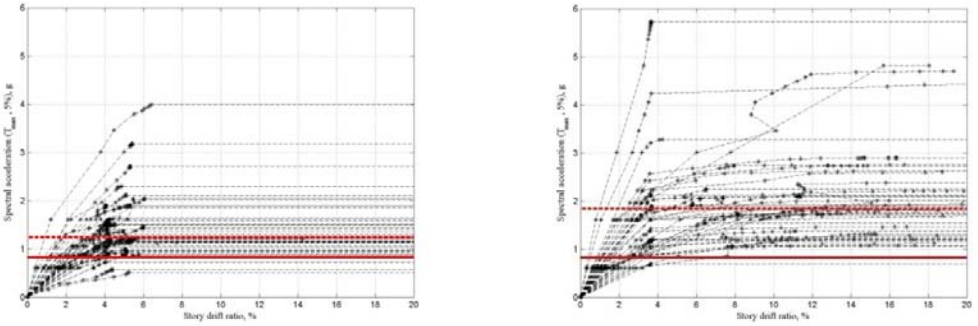

Static pushover curves

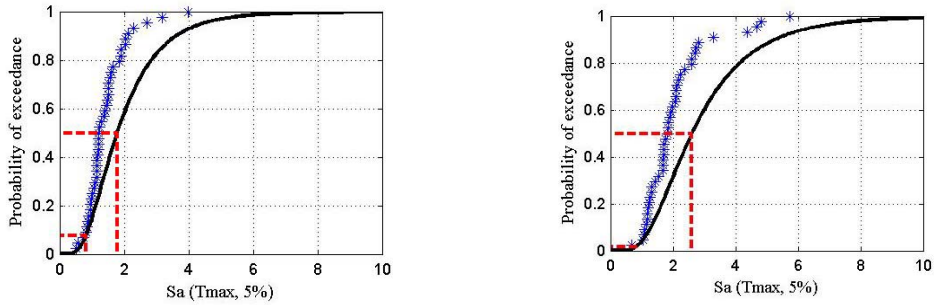

Fragility plots

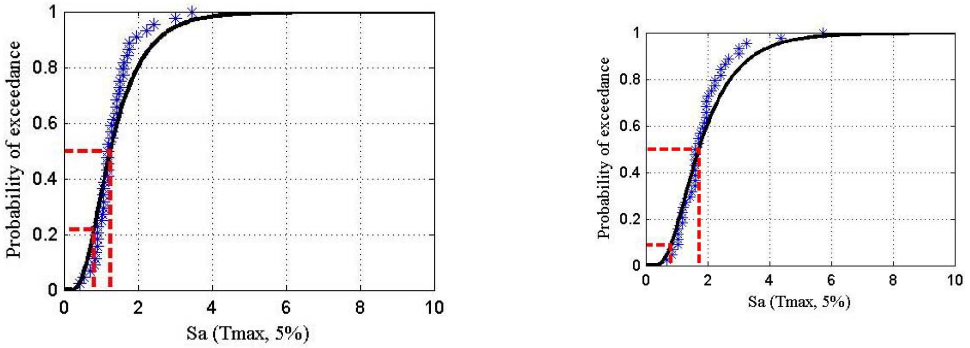

Damper force fragility

Figure 11. Analysis results

CONCLUSIONS

New steel buildings were designed using performance based engineering (PBE) and provisions of ASCE 7. SMRFs were used to provide strength; dampers were used to control story drifts. PBE design using dampers is superior to the conventional design. The demand on both structural and nonstructural components is reduced. To date, a model of viscous dampers with limit states has been formulated that includes damper limit states. Current research using IDA and limit states of dampers is currently underway. The outcome of this study will provide a more realistic assessment of the performance of moment frames with dampers. All the archetypes had significant margin against collapse and thus had satisfactory performance. When a damper factor of safety is included in design, additional protection for the structures and dampers is provided. As one of the research deliverables, pertinent information will be provided for the designers to assist in seismic design using this approach

ACKNOWLEDGEMENTS

The authors acknowledge financial support from Taylor Devices and Armor Steel. The technical assistance of Mr. Doug Taylor and Mr. John Metzger of Taylor Devices is also acknowledged.

REFERENCES

ASCE (2005), "ASCE 7-05: Minimum design load for buildings and other structures," American Society of Civil Engineers, Reston, VA

FEMA (2000), FEMA 350: Recommended Seismic Design Criteria for New Steel Moment Frame Buildings, Federal Emergency Management Agency, Washington DC.

Liel, A.B.., and Deierlein G.G., (2008), Assessing The Collapse Risk Of California's Existing Reinforced Concrete Frame, Structures: Metrics For Seismic Safety Decisions, John A. Blume Earthquake Engineering Center Report No. TR 166, Department of Civil Engineering, Stanford University.

Lignos, D. G.(2008), Sidesway Collapse Of Deteriorating Structural Systems Under Seismic Excitation, PhD dissertation, Department of Civil and Environmental Engineering, Stanford University.

Miyamoto, H.K., and Gilani, A.SJ. (2008), Design of a new steel-framed building using ASCE 7 damper provisions, ASCE Structures Congress, Vancouver, BC, SEI institute.

NEHRP (2009), "ATC 63, FEMA P695: Quantification of Building Seismic Performance Factors," Federal Emergency Management Agency, Washington, D.C.

PEER (2009a), Open System for Earthquake Engineering Simulation (OpenSees), McKenna, F., Fenves, G., et al, Pacific Earthquake Engineering Research center, University of California, Berkeley. Berkeley, CA.

PEER (2009b), PEER NGA, Records Pacific Earthquake Engineering Research center, University of California, Berkeley. Berkeley, CA.

Taylor (2009), Personal Communications

Vamvatsikos, D. and Cornell, A.C. (2004) Applied Incremental Dynamic Analysis, Earthquake Spectra, Volume 20, No. 2, pages 523–553, Earthquake Engineering Research Institute, Oakland, CA